MnO and NiO nanoparticles: synthesis and magnetic properties

Moumita Ghosh,[ab] Kanishka Biswas,[ab] A. Sundaresan[a] and C. N. R. Rao*[ab]

Received 22nd August 2005, Accepted 22nd September 2005
First published as an Advance Article on the web 13th October 2005
DOI: 10.1039/b511920k

Nanoparticles of MnO with average diameters in the 6–14 nm range have been prepared by the decomposition of manganese cupferronate in the presence of TOPO, under solvothermal conditions. Nanoparticles of NiO with average diameters in the 3–24 nm range have been prepared by the decomposition of nickel cupferronate or acetate under solvothermal conditions. The nanoparticles have been characterized by X-ray diffraction and transmission electron microscopy. Both MnO and NiO nanoparticles exhibit supermagnetism, accompanied by magnetic hysteresis below the blocking temperature (T_B). The T_B increases with the increase in particle size in the case of NiO, and exhibits the reverse trend in the case of MnO.

Introduction

Nanoparticles of transition metal oxides have been investigated by several workers in the last few years. Besides their structural aspects, magnetic properties of the oxide nanoparticles are of particular interest. Thus, it would be of value to know if the nanoparticles of antiferromagnetic oxides generally show evidence for ferromagnetic interaction at low temperatures, a behaviour that has been reported by a few workers.[1,2] A recent study of CoO nanoparticles has shown that small particles of less than 16 nm diameter exhibit magnetic hysteresis below a blocking temperature of $\sim$10 K.[3] We were interested to investigate nanoparticles of the binary metal oxides MnO and NiO, which are antiferromagnetic with Neél temperatures of 122 K and 523 K respectively.[4] There have been a few reports in the literature on MnO nanoparticles. Lee *et al.*[5] prepared MnO nanoparticles by the decomposition of $Mn_2(CO)_8$, but the product always contained Mn_2O_3 as an impurity. These workers, however, found ferromagnetic behaviour in the particles with an average diameter of around 5 nm. Yin and O'Brien[6] synthesized MnO nanocrystals capped with organic ligands by the decomposition of manganese acetate in a mixture of trioctylamine and oleic acid. These workers did not study the magnetic properties of the nanoparticles. Colloidal MnO nanoparticles, prepared by Seo *et al.*[7] by the decomposition of manganese acetylacetonate in oleylamine, showed divergence in the magnetization measured under zero-field-cooled (ZFC) and field-cooled (FC) conditions. Park *et al.*[8,9] prepared MnO nanospheres with diameters in the 5–40 nm range and nanorods of 7–10 nm diameter by the thermal decomposition of Mn-surfactant complexes in trioctylphosphine. These workers also observed divergence in the magnetization recorded under ZFC and FC conditions. We have prepared MnO nanoparticles by the decomposition of manganese cupferronate, $Mn(cup)_2$, in toluene in the presence of trioctylphosphine oxide (TOPO) under solvothermal conditions and obtained nanoparticles with diameters in the 6–14 nm range. The particles so-prepared had an organic coating and enabled a study of magnetic properties without any surface oxidation.

Small particles of NiO have been known to be superparamagnetic for some time.[10] Magnetic anomalies, such as low temperature hysteresis below a blocking temperature and divergence between the FC and ZFC magnetization data, on NiO nanoparticles have been reported.[2,11,12] The anomalies in the magnetic properties are attributed to uncompensated surface spins causing a change in the magnetic order in the nanoparticles.[1,12] NiO nanoparticles have been prepared by the decomposition of the hydroxide.[10,2,13] and by the oxidation of Ni nanoparticles[14] or by the decomposition of nickel oxalate.[15] We have prepared the nanoparticles of NiO of different diameters in the 3–24 nm range by the decomposition of nickel cupferronate, $Ni(cup)_2$, or nickel acetate in organic solvents under solvothermal conditions. The as-prepared particles have a protective organic coating. We have examined the magnetic properties of MnO and NiO nanoparticles, after characterizing them by X-ray diffraction and transmission electron microscopy.

Experimental

Manganese cupferronate, $Mn(C_6H_5N_2O_2)_2$, or $Mn(cup)_2$ was synthesized as follows.[16] 1 g (5.05 mmol) of $MnCl_2{\cdot}4H_2O$ was dissolved in 100 ml of milli-Q water and 1.56 g (10.05 mmol) of cupferron was dissolved in 50 ml of milli-Q water by sonication. The two solutions were cooled at 0 °C and the cupferron solution added dropwise to the $MnCl_2$ solution under vigorous stirring. After a few minutes, a pale yellow coloured product was obtained. It was filtered, washed thoroughly with milli-Q water and dried at room temperature overnight.

MnO nanoparticles were prepared by the decomposition of $Mn(cup)_2$ at 325 °C in toluene in the presence of trioctylphosphine oxide (TOPO) as the capping agent. In a typical reaction, 0.2 g (0.60 mmol) of $Mn(cup)_2$ and 0.95 g (2.45 mmol) of TOPO were taken in 10 ml of toluene and sealed in a

[a]*Chemistry and Physics of Materials Unit and CSIR Centre of Excellence in Chemistry, Jawaharlal Nehru Centre for Advanced Scientific Research, Jakkur P. O., Bangalore-560064, India. E-mail: cnrrao@jncasr.ac.in; Fax: (+91) 80 22082760*
[b]*Solid State and Structural Chemistry Unit, Indian Institute of Science, Bangalore-560012, India*

stainless steel Swagelok autoclave of 20 ml capacity. The autoclave was kept inside a preheated tube-furnace at 325 °C for 2 h, and was then allowed to cool to room temperature. A brownish black solution was obtained as the product. To this solution, excess ethanol was added and kept overnight. Black coloured TOPO-capped MnO nanoparticles (14 nm diameter) obtained as a solid residue were washed several times with ethanol and acetone.

To vary the particle size of MnO, the concentration of $Mn(cup)_2$, and/or the concentration of TOPO as well as the reaction time were varied, keeping the amount of toluene and the filling fraction of the autoclave constant. The nanoparticles of different diameters were obtained as follows: 6 nm, 0.005 g (0.015 mmol) of $Mn(cup)_2$, 0.045 g (0.012 mmol) of TOPO, 325 °C, 2 h 30 min; 8.5 nm, 0.025 g (0.075 mmol) of $Mn(cup)_2$, 0.18 g (0.046 mmol) of TOPO, 325 °C, 2 h; 10 nm, 0.01 g (0.03 mmol) of $Mn(cup)_2$, 0.09 g (0.024 mmol) of TOPO, 340 °C, 2 h; 14 nm, 0.2 g (0.60 mmol) of $Mn(cup)_2$, 0.95 g (2.45 mmol) of TOPO, 325 °C, 2 h. The nanoparticles could be readily redispersed in toluene by sonication.

Nickel cupferronate, $Ni(C_6H_5N_2O_2)_2$, or $Ni(cup)_2$, was prepared as follows. 2 g of $Ni(OAc)_2{\cdot}4H_2O$ was dissolved in 150 ml of milli-Q water (0.05 M), and 2.5 g of cupferron dissolved in 100 ml of milli-Q water (0.16 M) by sonication. The two solutions were cooled to 0 °C and the cupferron solution added dropwise to the $Ni(OAc)_2$ solution under vigorous stirring. After a few minutes, the solution became turbid, indicating the formation of complex. It took another 30 min for completion of the reaction. Before filtration, the product was kept at 0 °C for 1 h. The product was filtered and washed with milli-Q water and dried at room temperature.

NiO nanoparticles were synthesized in toluene under solvothermal conditions as follows. In a typical reaction, 0.05 g (0.15 mmol) of $Ni(cup)_2$ were taken in 48 ml of toluene and subjected to sonication for 10 min. The resulting green coloured solution was sealed in a Teflon-lined stainless steel autoclave of 80 ml capacity (allowing 70% filling fraction) and the autoclave was placed inside a air-oven preheated at 240 °C for 8 h. The autoclave was allowed to cool to room temperature. A brownish coloured solid dispersed in toluene was obtained as the product. Addition of methanol to this toluene dispersion allowed the solid to settle down. The product was washed with methanol by sonication followed by centrifugation. The sample was dried in an air-oven at 50 °C for 1 h. The average diameter of the particle obtained under these preparative conditions was 3 nm. In order to prepare 7 nm NiO nanoparticles, we used 0.4 g (1.2 mmol) of $Ni(cup)_2$ in 48 ml of toluene and carried out the reaction for 24 h, keeping the temperature and filling fraction of the autoclave as constant. In addition to the NiO nanoparticles described above, trioctylphosphine oxide (TOPO)-capped NiO nanoparticles of 3 nm average diameter were prepared by taking 0.5 g (1.5 mmol) of $Ni(cup)_2$ in 1.5 mmolar toluene solution of TOPO.

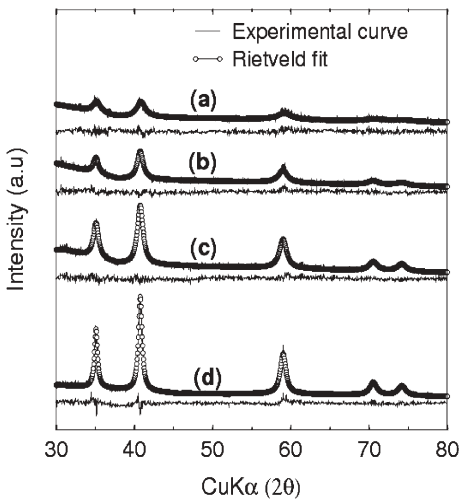

Fig. 1 XRD patterns of the MnO nanoparticles with average diameters of (a) 6, (b) 8.5, (c) 10 and (d) 14 nm along with the Rietveld fits. Difference patterns are shown below the observed patterns.

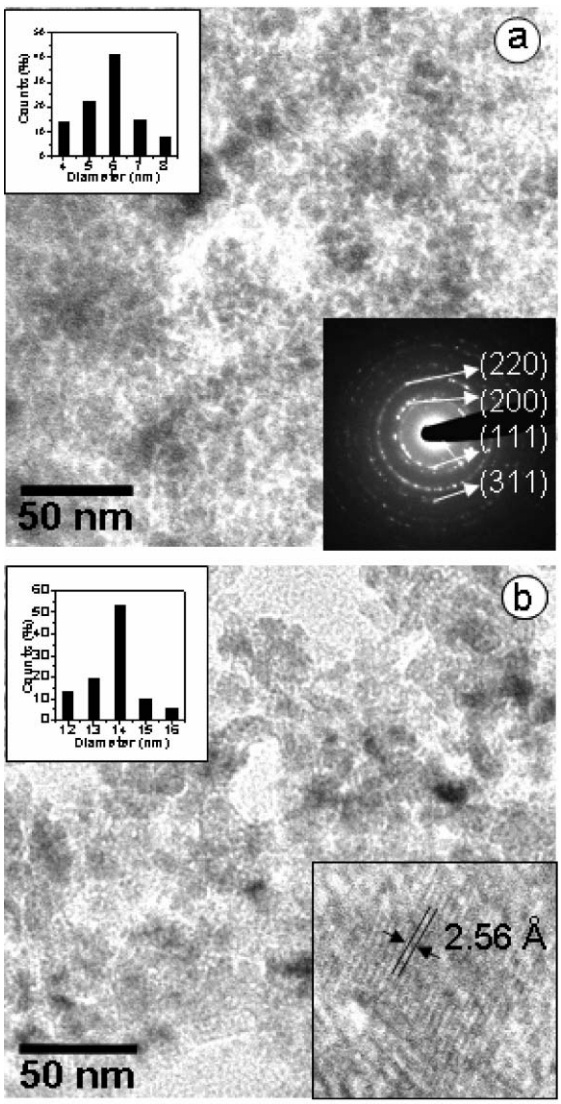

Fig. 2 TEM images of (a) 6 nm and (b) 14 nm particles of MnO. Insets in (a) show the SAED pattern and the size distribution histogram. Insets in (b) show the single particle HREM image and the size distribution.

We have also prepared NiO nanoparticles by the solvothermal decomposition of $Ni(OAc)_2$ using toluene as the solvent in a stainless steel Swagelok autoclave of 20 ml capacity. To prepare 12 nm NiO particles, 0.1 g (0.4 mmol) of $Ni(OAc)_2{\cdot}4H_2O$ was taken in 10 ml of toluene and the reaction mixture sealed in a Swagelok autoclave of 20 ml capacity. The autoclave was kept inside a preheated tube furnace at 250 °C. The reaction was carried out for 3 h. A moss green coloured, toluene-insoluble solid residue was obtained as the product. NiO particles of 24 nm diameter were prepared by taking 0.5 g (2.01 mmol) of $Ni(OAc)_2{\cdot}4H_2O$ in 10 ml toluene, and carrying out the reaction at 335 °C for 1 h.

The nanoparticles were characterized by powder X-ray diffraction (XRD) using a Phillips X'Pert diffractometer employing the Bragg–Brentano configuration using CuKα radiation with the scan rate of $0.16^\circ\ 2\theta\ min^{-1}$. The data were then rebinned into 0.05° steps. For transmission electron microscopy (TEM), toluene dispersions of the samples were dropped onto the holey carbon-coated Cu grids, and the grids were allowed to dry in the air. The grids were examined using a JEOL (JEM3010) microscope operating with an accelerating voltage of 300 kV. Thermogravimetric analysis (TGA) was carried out using a Mettler Toledo Thermal Analyser. Powder samples of the as-prepared nanoparticles were subjected to magnetic characterization using the VSM in PPMS (Physical Property Measurement System).

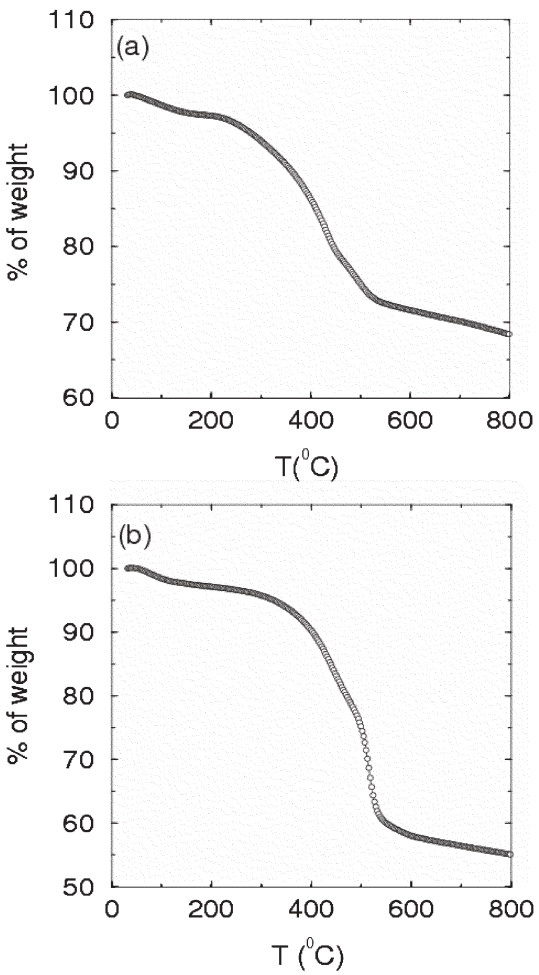

Fig. 3 TGA curves of (a) 14 nm TOPO-capped MnO nanoparticles and (b) 3 nm uncapped NiO nanoparticles. The experiments were carried out in a nitrogen atmosphere at a heating rate of 10 °C min^{-1}.

Results and discussion

MnO

In Fig. 1, we show the X-ray diffraction patterns of MnO nanoparticles of four different sizes. Fig. 1 also gives the Rietveld profile fits along with the difference patterns obtained by using the Rietveld XND code.[17] The patterns could be indexed with the *Fm*3*m* space group (JCPDS no 07-0230). By making the use of the line widths from the Rietveld fits, the average particle sizes were estimated by using the Scherrer formula. The particle sizes are indicated in Fig. 1. The cubic lattice parameter of the 8.5 and 14 nm particles are 4.429 and 4.428 Å respectively. The TEM images of the MnO nanoparticles with average diameters of 6 and 14 nm are shown in Fig. 2(a) and (b), respectively. An indexed selected area electron diffraction (SAED) pattern of the 6 nm sample is shown in the inset of Fig. 2(a). The particle size distributions are shown as insets in Fig. 2. Most of the particles in Fig. 2(a) and (b) have diameters of 6 and 14 nm respectively, which compare well with the values calculated from the XRD

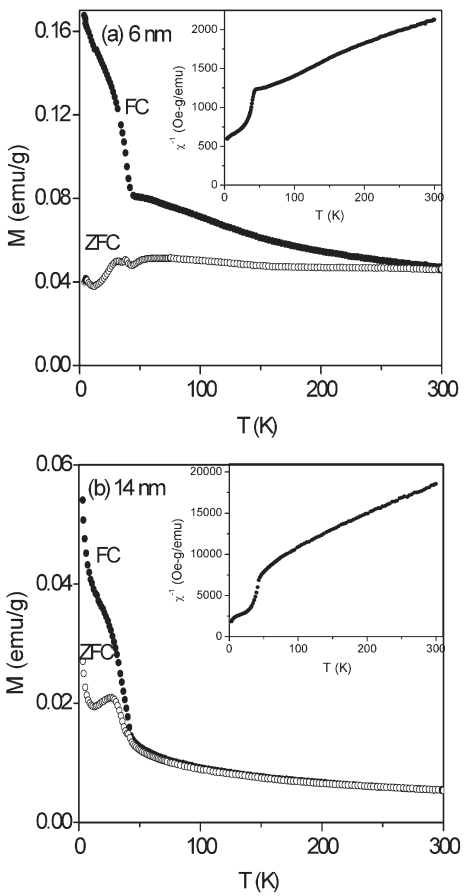

Fig. 4 Magnetization *vs.* temperature curves of (a) 6 nm and (b) 14 nm MnO particles under FC and ZFC conditions using a magnetic field of 100 Oe. The insets show inverse susceptibility *vs.* temperature curves.

patterns. We show an HREM image of a 14 nm MnO nanoparticle as an inset in Fig. 2(b). The lattice spacing of 2.56 Å in the image corresponds to the interplanar distance between (111) planes. The images of the particles are not as good as one would desire because of the organic coating on the particles. The presence of such an organic coating is evidenced from the TGA curve shown in Fig. 3(a), for the 14 nm MnO nanoparticles. The organic coating is removed around 400 °C. The presence of the organic coating helps to avoid oxidation of the MnO nanoparticles.

In Fig. 4(a) and (b), we show the magnetization data of two samples with average diameters of 6 and 14 nm respectively. The FC and ZFC data show divergence at low temperatures as indeed found in the case of other oxide nanoparticles. The magnetization in the FC data shows a marked increase at low temperatures, where a shoulder like feature is also evident. The ZFC data clearly show maxima corresponding to blocking temperatures (T_B) of the nanoparticles. The T_B of the 6 nm particle is higher than that of the 14 nm particles indicating an inverse relationship. A similar dependence has been noticed earlier.[7] The insets in Fig. 4(a) and (b) represent the inverse susceptibility (χ^{-1}) *vs.* temperature data. The magnetic moments estimated from the χ^{-1} data in the high temperature data are around 4 μ_B, a value close to that expected for MnO. The Curie–Weiss temperatures (Θ_p) obtained from the extrapolation of the high-temperature inverse susceptibility data are −202 and −365 K respectively for the 6 nm and 14 nm samples. The negative sign of Θ_p indicates predominant antiferromagnetic interaction. The value of Θ_p decreases with the increase in particle size, probably because the ferromagnetic interaction decreases with the increase in particle size. Accordingly, the value of the magnetization of the 6 nm particles is always higher than that of the 14 nm particles. In Fig. 5(a), we show the variation of magnetization with field at 5 K and 50 K for the 6 nm particles to reveal the occurrence of hysteresis at low temperatures, the H_c value being 1750 Oe at 5 K. At high temperatures ($T > T_B$), the hysteresis disappears.

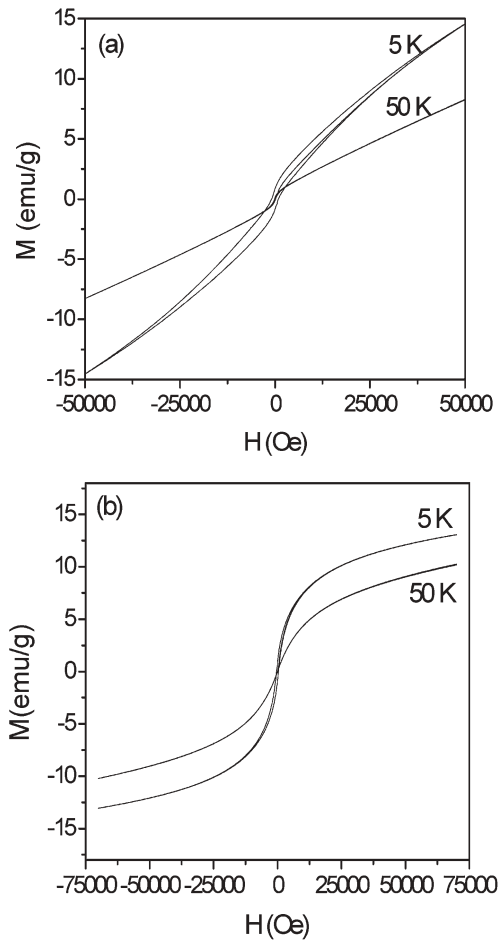

Fig. 5 Field dependence of magnetization of the (a) 6 nm MnO nanoparticles and (b) 3 nm NiO nanoparticles at 5 K and 50 K. Notice the absence of saturation and the disappearance of hysteresis at high temperatures.

NiO

In Fig. 6, we show the X-ray diffraction patterns of four different sizes of NiO nanoparticles. The Rietveld fitting of the profiles was carried out using the Rietveld XND code.[17] The diffraction profiles could be indexed on the *Fm*3*m* space group (JCPDS no 47-1049). The particles sizes were estimated using the Scherrer formula by taking the average of three main line-widths obtained from the Rietveld fitted profiles. The lattice parameters obtained from the Rietveld fits are 4.178 Å, 4.182 Å, 4.192 Å and 4.211 Å respectively for the 24, 12, 7 and 3 nm nanoparticles, reflecting a slight increase in the lattice parameter with the decrease in particle size. The presence of a passive organic coating on the surfaces of the particles is evidenced from the TGA curve shown in Fig. 3(b). The coating is removed around 400 °C, accompanied by the partial reduction of NiO to Ni metal. In Fig. 7(a) and (b), we show the TEM images of the NiO nanoparticles with average diameters of 3 and 7 nm respectively, along with the size distributions.

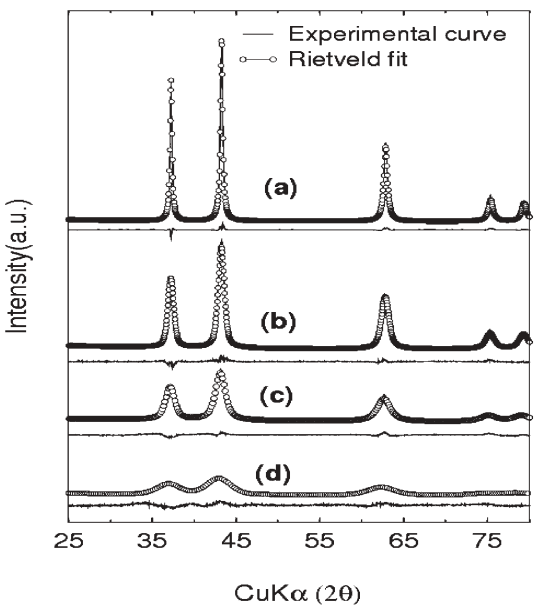

Fig. 6 XRD patterns of the NiO nanoparticles with average diameters of (a) 24, (b) 12, (c) 7 and (d) 3 nm along with the Rietveld fits. The difference patterns are shown below the corresponding observed patterns.

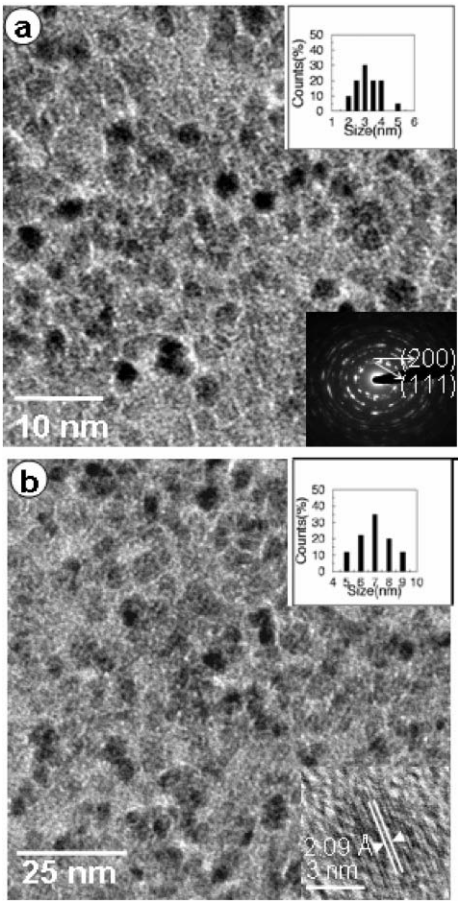

Fig. 7 TEM images of (a) 3 and (b) 7 nm NiO nanoparticles. The insets show the histograms of the particle size distributions (upper panels). The lower panel in (a) shows the SAED pattern. The HREM image of a single NiO nanoparticle of 6 nm is shown in the lower panel in (b).

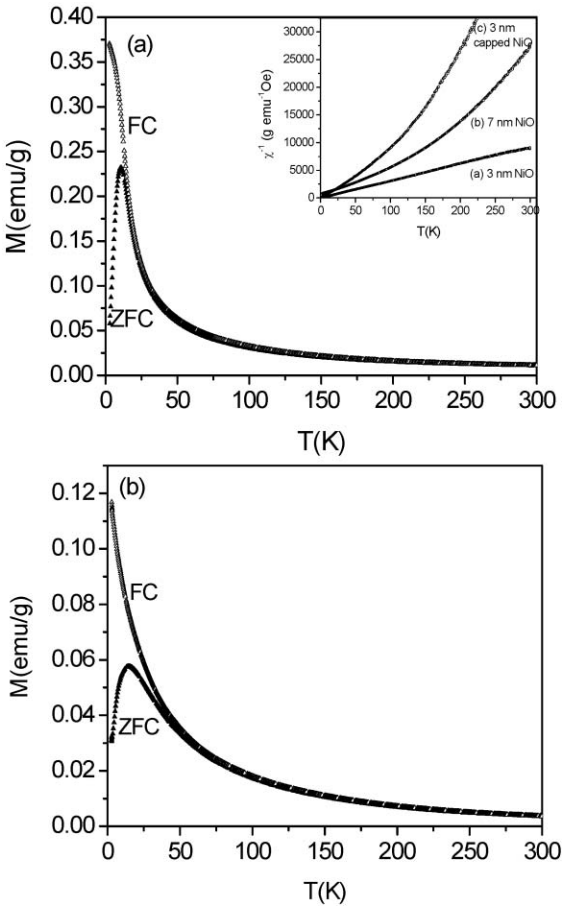

Fig. 8 The temperature dependence of dc magnetization of (a) 3 nm and (b) 7 nm NiO nanoparticles under ZFC and FC conditions (H = 100 Oe). The inset shows the inverse susceptibility *vs.* temperature curves of the (a) 3 nm and (b) 7 nm particles; (c) shows the data for TOPO-capped 3 nm NiO nanoparticles.

The average particle sizes estimated from the TEM are consistent with the values obtained from the XRD patterns. The indexed SAED pattern shown in Fig. 7(a) suggests the particles to be crystalline. The pattern could be indexed on the basis of the *Fm*3*m* space group. The HREM image of a 6 nm NiO particle, shown as an inset in Fig. 7(b), shows a lattice spacing of 2.09 Å, corresponding to the interplannar distance between the (100) planes.

We show the temperature dependence of magnetization curves of 3 and 7 nm NiO nanoparticles under ZFC and FC conditions in Fig. 8(a) and (b) respectively. We observe a divergence between the ZFC and FC data, as with the MnO nanoparticles. The ZFC data show maxima corresponding to the blocking temperature (T_B). The T_B increases with the particle size, the values being 10 K and 15 K respectively for the particles with the average diameters of 3 nm and 7 nm. Such a proportionality between T_B and particle size is expected and has been noticed earlier in some cases.[7,14] We show the inverse susceptibility (χ^{-1}) data in the inset of Fig. 8(a). The magnetic moments estimated from the inverse susceptibility data in the high temperature regime are around 3 μ_B, which is close to the value expected for Ni^{2+}. We notice that the Curie–Weiss temperature is close to zero for the 3 nm particles and negative for the 7 nm particles. The value of the magnetization of the 3 nm particles is also higher than that of the 7 nm particles. The magnetic hysteresis curves for the 3 nm NiO particles are shown in Fig. 5(b). The hysteresis curve at 5 K is associated with a H_c value of 350 Oe. The hysteresis is absent at 50 K. We have measured the magnetic susceptibility of the 3 nm NiO particles capped with TOPO as well. These capped nanoparticles exhibit a lower magnetization than the NiO nanoparticles prepared in the absence of TOPO. The Curie–Weiss temperature of the TOPO-capped nanoparticles is near zero.

Conclusions

MnO and NiO nanoparticles (both in the *Fm*3*m* space group) of different sizes have been prepared by the decomposition of the metal cupferronate or the acetate in organic solvents under solvothermal conditions. Magnetic properties of the well-characterized nanoparticles of these antiferromagnetic oxides reveal the presence of superparamagnetism (often mentioned as ferromagnetic interactions in the literature), as evidenced by the increasing magnetization with decreasing size as well as the magnetic hysteresis at low temperatures.

Interestingly, the blocking temperature (T_B) increases with the increase in particle size as expected from theory in the case NiO nanoparticles, but shows the opposite relation in the case of MnO nanoparticles. It is not clear why such an inverse relation between T_B and particle size manifests itself. It is noteworthy that supermagnetism at low temperatures is the general feature of small nanoparticles of transition metal oxides, which are otherwise antiferromagnetic with fairly high Néel temperatures.

Acknowledgements

The authors thank Professor E. V. Sampthkumaran for preliminary magnetic measurements.

References

1 R. H. Kodama, *J. Magn. Magn. Mater.*, 1999, **200**, 359.
2 S. A. Makhlouf, F. T. Parker, F. E. Spada and A. E. Berkowitz, *J. Appl. Phys.*, 1997, **81**, 5561.
3 M. Ghosh, E. V. Sampatkumaran and C. N. R. Rao, *Chem. Mater.*, 2005, **17**, 2348.
4 C. N. R. Rao and B. Raveau, *Transition Metal Oxides*, 2nd edn, Wiley-VCH, Germany, 1995.
5 G. H. Lee, S. H. Huh, J.W. Jeong, B. J. Choi, S. H. Kim and H.-C. Ri, *J. Am. Chem. Soc.*, 2002, **124**, 12094.
6 M. Yin and S. O'Brien, *J. Am. Chem. Soc.*, 2003, **125**, 10180.
7 W. S. Seo, H. H. Jo, K. Lee, B. Kim, S. J. Oh and J. T. Park, *Angew. Chem., Int. Ed.*, 2004, **43**, 1115.
8 J. Park, E. Kang, C. J. Bae, J.-G. Park, H.-J. Noh, J.-Y. Kim, J.-H. Park, H. M. Park and T. Hyeon, *J. Phys. Chem. B*, 2004, **108**, 13594.
9 J. Park, K. An, Y. Hwang, J. G. Park, H. J. Noh, J. Y. Kim, J. H. Park, N. M. Hwang and T. Hyeon, *Nature Mater.*, 2004, **3**, 891.
10 J. T. Richardson, D. I. Yiagas, B. Turk, K. Forster and M. V. Twigg, *J. Appl. Phys.*, 1991, **70**, 6977.
11 F. Bødker, M. F. Hansen, C. B. Koch and S. Mørup, *J. Magn. Magn. Mater.*, 2000, **221**, 32.
12 R. H. Kodama, S. A. Makhlouf and A. E. Berkowitz, *Phys. Rev. Lett.*, 1997, **79**, 1393.
13 C. L. Carnes, J. Stipp and K. J. Klabunde, *Langmuir*, 2002, **18**, 1352.
14 B. J. Park, E. Kang, S. Uk. Son, H. M. Park, M. K. Lee, J. Kim, K. W. Kim, H.-J. Noh, J.-H. Park, C. J. Bae, J.-G. Park and T. Hyeon, *Adv. Mater.*, 2005, **17**, 429.
15 W. Xiong, J. Song, L. Gao, J. Jin, H. Zheng and Z. Zhang, *Nanotechnology*, 2005, **16**, 37.
16 K. Tamaki and N. Okabe, *Acta Crystallogr., Sect. C*, 1996, **52**, 1612.
17 J.-F. Bérar and P. Garnier, *NIST Spec. Publ.*, 1992, **846**, 212.